JOURNAL OF GEOPHYSICAL RESEARCH, VOL. 106, NO. A12, PAGES 30,371–30,380, DECEMBER 1, 2001

Inferring *E* region electron density profiles at Jicamarca from Faraday rotation of coherent scatter

D. L. Hysell

Department of Physics and Astronomy, Clemson University, Clemson, South Carolina

J. L. Chau

Radio Observatorio de Jicamarca, Instituto Geofísico del Perú, Lima, Perú

Abstract. A new technique for measuring *E* region plasma density profiles in the equatorial electrojet using a bistatic coherent scatter radar is described. The technique utilizes the Faraday rotation of the obliquely and coherently scattered signal. Plasma density versus altitude is inferred from the rate of Faraday rotation as a function of range and elevation angle. A narrow beam width is required to minimize returns from unwanted azimuths, but this can be achieved in a bistatic experiment using relatively small antenna arrays with widely spaced elements. We give a sample time sequence of daytime electron density profiles that were measured with the new technique at altitudes between 95 and 110 km. Scatter from pure two-stream waves makes it possible to measure both the bottomside and topside density profiles during the day. The importance of this new technique becomes evident when one realizes that only a few rocket flights have provided density profiles through these altitudes at the magnetic equator; the region has been inaccessible to any remote sensing technique until now.

1. Introduction

In this paper we report on a new remote sensing technique designed to measure electron density profiles in the equatorial *E* region. As we discuss below, this region is generally inaccessible to incoherent scatter radars and ionosondes and remains poorly characterized as a result. Our main sources of information about the region have been sounding rockets launched during international campaigns. A review of these experiments was given by *Pfaff et al.* [1987a, 1997]; *Pfaff* [1991] and references therein. These campaigns provide brief, sporadic glimpses of the structure of the ionization but reveal little about how the structure evolves over time. Consequently, little is known about the local time and seasonal variability of the equatorial *E* region. The shape of the density profile at night is particularly enigmatic, and even the daytime profile shape as a function of local time is not well established.

The inaccessibility of the equatorial *E* region inhibits progress in a number of lines of research in equatorial aeronomy and plasma physics. Ionospheric electric field estimates based on magnetometer data taken in the vicinity of the equatorial electrojet suffer from uncertainties related to uncertainties in the *E* region densities. These uncertainties hinder efforts to model quantitatively and self-consistently the electrojet current system [*Forbes*, 1981]. Likewise, a quantitative understanding of the behavior, growth, and propagation of gradient drift waves in the electrojet will not be forthcoming until radar observations of the waves and of the underlying plasma density profiles and gradients are available simultaneously [*Ronchi*, 1990]. Ionization in the *E* region is thought to suppress the formation of *F* region irregularities by loading magnetic field lines. While this principle is widely accepted, it cannot be quantified experimentally without access to *E* region density profile measurements [*Woodman*, 1994]. Recently, *Fesen et al.* [2000] reported that the National Center for Atmospheric Research (NCAR) Thermosphere Ionosphere Electrodynamic General Circulation Model (TIEGCM) could not reproduce the well-known phenomenon of the prereversal enhancement of the zonal electric field unless *E* region densities were reduced to values well below those predicted by the empirical international reference ionosphere model (IRI). This finding could have substantial bearing on the cause of variability in the postsunset equatorial *F* region, but we cannot assess its significance without first knowing what densities are realistic.

In middle and high latitudes, *E* region density profiles are routinely measured using conventional incoherent scatter radar techniques. Near the magnetic equator, however, intense radar clutter arising from plasma irregularities in the electrojet generally makes incoherent scatter impossible to detect. Even when the antenna pattern of the Jicamarca Radio Observatory is directed obliquely to the geomagnetic field, intense field-aligned backscatter from the *E* region enters through the antenna sidelobes, causing se-

Paper number 2000JA001101.
0148-0227/01/2000JA001101$09.00

vere interference. This interference subsides briefly around dawn and dusk, when the zonal ionospheric electric field reverses and the irregularities momentarily vanish. However, the interference-free intervals are usually too brief to exploit practically with incoherent scatter techniques, and correlative studies between the irregularities and the density profile they embed are not possible in any case.

Like the incoherent scatter radar, the ionosonde at Jicamarca also suffers from interference from coherent scatter in E region range gates. Reflection goes smoothly into scattering in ionograms measured at Jicamarca, and, at present, no model exists for inverting ionograms that include the effects of coherent scatter and reflection (R. F. Woodman, personal communication, 1999). Furthermore, ionosondes cannot measure density profiles in the topside E and valley regions.

Our new technique takes advantage of coherent scatter from electrojet irregularities to estimate the E region density profile. It does so by measuring the Faraday rotation of the scattered signal. Faraday rotation occurs in proportion to the electron density along the signal ray path. Differences in the Faraday angle from one radar range gate to the next are indicative of the plasma density at a given altitude.

F region electron density profiles have been inferred from the Faraday rotation of incoherent backscatter at Jicamarca for many years [*Farley*, 1969a; *Pingree*, 1990; *Aponte et al.*, 1997]. In these experiments the main beam of the antenna is directed a few degrees off perpendicular to $\mathbf{B}$, and Faraday rotation rates on the order of 2π radians per hundred kilometers are measured near the F peak. If this technique were to be adapted to E region field-aligned coherent backscatter, however, the rotation rate would decrease drastically, and measuring density profiles in the relatively thin and rarefied E layer would be difficult in practice. This is because the rotation rate becomes small when the radar wave vector is close to perpendicular to $\mathbf{B}$. (In fact, the Faraday rotation phenomenon takes on a different character for perpendicular propagation, as the magnetoionic modes transition from elliptic to linear polarizations [*Ratcliffe*, 1959, 1972].) Here we sidestep complications associated with transverse propagation by employing a bistatic radar system. With a bistatic radar the scattering wave vector can lie perpendicular to $\mathbf{B}$ even when the radar wave vector is always oblique to $\mathbf{B}$. Using a small, bistatic, 50-MHz radar system, we detect more than 1 rad. of Faraday rotation for radar signals passing through the daytime E layer.

The paper is organized as follows. We begin with a description of the new technique and address some technical issues unique to it. We then present some preliminary data, taken in Peru in September 2000. These data are compared to density profiles from a sounding rocket experiment and from the IRI model. Finally, we summarize the significance of this work and outline its future direction.

2. Technique Description

Figure 1 is a representation of the bistatic coherent scatter experiment. Transmitting and receiving stations are operated from Paracas and Jicamarca, Peru, respectively. The

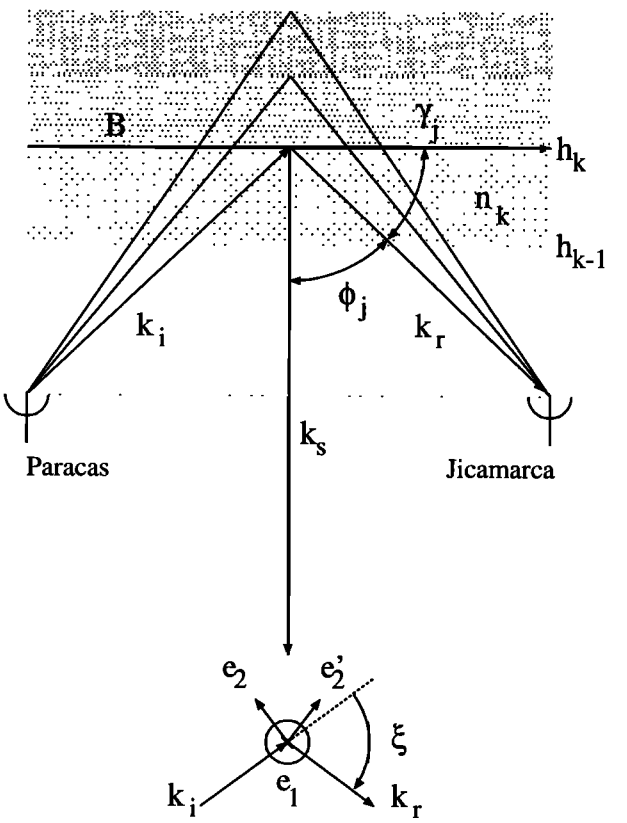

Figure 1. Schematic diagram depicting the bistatic radar experiment. The transmitter (receiver) is located at Paracas (Jicamarca). See text for symbol definitions.

electrojet current and associated E layer irregularities exist in between where the geomagnetic field is nearly horizontal. (Note that the geomagnetic field $\mathbf{B}$ does not actually lie in the plane of Figure 1.) In Figure 1, $\mathbf{k}_i$ and $\mathbf{k}_r$ are the incident and scattered radar signal free-space wave vectors. Figure 1 illustrates that whereas these vectors have significant components parallel to the geomagnetic field, the scattering wave vector $\mathbf{k}_s = \mathbf{k}_r - \mathbf{k}_i$ lies perpendicular to $\mathbf{B}$. This geometry is necessary for the simultaneous detection of coherent scatter and substantial Faraday rotation.

A horizontally polarized signal is transmitted from Paracas which propagates into the E region and undergoes Faraday rotation. Just prior to scattering, the signal is no longer horizontally polarized, and the incident electric field has both horizontal and vertical linear components transverse to $\mathbf{k}_i$. Define $\mathbf{e}_1$ and $\mathbf{e}_2$ as unit vectors transverse to $\mathbf{k}_i$ with $\mathbf{e}_1$ oriented horizontally. Also, define η as the angle the linearly polarized wave makes with $\mathbf{e}_1$ just prior to scattering. Consider next that a linearly polarized plane wave can be decomposed into left and right circularly polarized waves, and the circularly polarized electric field components of the signal prior to scattering can therefore be represented as

$$\mathbf{E}_{\pm}(\mathbf{x},t) = E_o(\mathbf{e}_1 \pm i\mathbf{e}_2)e^{i(\mp\eta - n_{\pm}\mathbf{k}_i\cdot\mathbf{x}+\omega t)},$$

where E_o is a real constant, $\mathbf{x}$ is the displacement from the scattering site, and $n_{\pm}$ refers to the indices of refraction for the left and right circularly polarized waves. For propagation

in the quasi-longitudinal limit with $\mathbf{k} \cdot \mathbf{B} > 0$, we identify ordinary and extraordinary modes with left and right circularly polarized waves, respectively, with the reverse holding for propagation with $\mathbf{k} \cdot \mathbf{B} < 0$. The differences in the indices of refraction for the magnetoionic modes give rise to Faraday rotation. Note that the Faraday angle θ, the difference in the phases of the left and right circularly polarized waves, is equal to 2η just prior to scattering.

The electric field scattered by the E region electrons is

$$\mathbf{E}'(\mathbf{R}) = -\frac{e}{R^3 c^2}\mathbf{R} \times (\mathbf{R} \times \dot{\mathbf{v}}),$$

where $\mathbf{R}$ is the vector displacement between the electron and the observer and $\dot{\mathbf{v}}$ is the electron acceleration induced by the incident field [*Jackson*, 1975]. Since $\dot{\mathbf{v}}$ is parallel to the incident electric field and $\mathbf{R}$ is parallel to $\mathbf{k}_r$, the component of the incident electric field parallel to $\mathbf{e}_1$ will remain parallel to $\mathbf{e}_1$ after scattering while the component parallel to $\mathbf{e}_2$ will become parallel to $\mathbf{e}_2'$, where $\mathbf{e}_2'$ is a unit vector normal to $\mathbf{e}_1$ and $\mathbf{k}_r$. Furthermore, the latter component will become modified by a factor of $\cos(\xi)$, where ξ is the angle between $\mathbf{k}_i$ and $\mathbf{k}_r$. The scattered signal components then become

$$\mathbf{E}'_{\pm}(\mathbf{x}, t) \propto E_o[\mathbf{e}_1 \pm i\cos(\xi)\mathbf{e}_2']e^{i(\mp\eta - n_{\pm}\mathbf{k}_r \cdot \mathbf{x} + \omega t)}.$$

The two oppositely polarized components of the scattered signal will, in general, be elliptically polarized with the same (different) sense of rotation as the incident signal components for acute (obtuse) scattering angles. However, the sum of the two components will remain a linearly polarized signal, again expressible as the sum of two circularly polarized waves:

$$\mathbf{E}'_{\pm}(\mathbf{x}, t) \propto E_o(\mathbf{e}_1 \pm i\mathbf{e}_2')e^{i(\mp\eta' - n_{\pm}\mathbf{k}_r \cdot \mathbf{x} + \omega t)}, \quad (1)$$

where $\eta' = \tan^{-1}[\tan(\eta)\cos\xi]$ is the angle the signal polarization makes with $\mathbf{e}_1$ immediately after scattering. The Faraday angle will be $\theta' = 2\eta'$ after scattering and will continue to change as the signal propagates back through the ionosphere toward the receiver. (The factor of 2 here again comes from differencing two equal and opposite values of η'.) For scattering at right angles (the Brewster angle) the scatter will be horizontally polarized initially. In our experiments the scattering angle is acute below 110 km, where it is precisely a right angle. Note that if the direction of propagation with respect to $\mathbf{B}$ changes after scattering, so too does the identification between right and left circularly polarized waves and the X and O modes. In the case of our experiments the identification always remains the same.

In the monostatic incoherent scatter Faraday rotation experiments performed at Jicamarca, independently transmitted left and right circularly polarized waves propagate with different indices of refraction and different phase speeds upward through the ionosphere. Upon scattering, the left circularly polarized wave converts to a right circularly polarized wave and vice versa, and the accumulated Faraday angle θ undergoes a change of sign. (The sign change is consistent with the definitions used above and reflects the fact that the coordinate system against which the Faraday angle is defined here is reoriented upon scattering.) Furthermore, the identification of right and left circular polarizations with the particular magnetoionic modes is reversed for the incident and backscattered signals. Consequently, as the scattered wave propagates back through the ionosphere, the magnitude of the Faraday angle continues to increase rather than returning to zero. Rotations incurred on the upward and downward trips contribute equally to the Faraday angle measured on the ground. Another way of viewing this is that the sense of rotation of the linearly polarized wave as viewed from an observer on the ground is the same on the upward and downward trips, controlled by resonant interactions between the wave and gyrating charged particles.

The bistatic technique utilizing scatter from field-aligned irregularities is more complicated than the monostatic experiment just described, both because of the range of shifts that the Faraday angle can undergo upon scattering (i.e., $\theta \rightarrow \theta'$) and because the identification of left and right circular polarizations with particular magnetoionic modes does not change upon scattering even though the polarizations themselves reverse in the case of scattering through obtuse angles. Because the scattering in our experiment is through nearly right angles, the radar signal is nearly horizontally polarized by the scattering, and the majority of the Faraday rotation detected by the receiver will be due to plasma encountered by the signal on the downward trip. A correction for rotation incurred up through the moment of scattering must nonetheless be applied since the algorithm for estimating electron densities is sensitive to small changes in the Faraday angle.

2.1. Density Profile Inference

Special care is needed when analyzing data from a bistatic radar when the distance between the receiver and the transmitter is comparable to the altitude of the scatterers. In Figure 1, ϕ_j is the zenith angle of the scattered ray associated with range gate j, and γ_j is the angle between the ray and the geomagnetic field. (Here we take $\mathbf{B}$ to be uniform.) Let h_k be the altitude for scatter falling into range gate k, so that $dh_k = h_k - h_{i-k}$. Further, take the plasma density to be horizontally stratified with n_k being the average density in the layer dh_k.

The phase difference between left and right circularly polarized radio waves passing through a magnetized plasma can be expressed compactly as

$$d\theta = \frac{4.72}{f_{\mathrm{MHz}}^2} B n_e \cos(\gamma) dl, \quad (2)$$

where the units of electron density (n_e), path length (dl), magnetic induction (B), and frequency (f) are 10^6 cm^{-3}, meters, Gauss, and megahertz, respectively. In writing (2) we have invoked the quasi-longitudinal approximation, which is appropriate for oblique propagation for radar frequencies well in excess of the electron gyrofrequency [*Booker*, 1984; *Budden*, 1988]. The approximation is tantamount to regarding the magnetoionic normal modes as being precisely circularly polarized. Neglecting the constants in (2), we can write the differential Faraday rotation for the

signal propagating along ray j downward through altitudes in dh_k as

$$d\theta_{jk} \propto n_k \cos(\gamma_j) \sec(\phi_j) dh_k,$$

where $\sec(\phi_j)dh_k$ is the path length taken by the ray in traversing dh_k, a slab of plasma with ionization density n_k. Note that ϕ_j is different for different scattering altitudes. The total Faraday rotation incurred along the ray propagating downward from the altitude h_j where scattering took place is then

$$\theta_j \propto \cos(\gamma_j) \sec(\phi_j) \sum_{k=1}^{j} n_k dh_k + C. \quad (3)$$

Here an arbitrary constant C has been introduced to represent phase delays due to unequal cable lengths or other asymmetries in the receiver system. In order to determine the plasma density at the altitude h_j, we compute the difference

$$n_j \propto \frac{1}{dh_j} \left(\frac{\theta_j - C}{\cos(\gamma_j)\sec(\phi_j)} - \frac{\theta_{j-1} - C}{\cos(\gamma_{j-1})\sec(\phi_{j-1})} \right).$$

It is important to note that the constant C does not vanish from this calculation. It will be expedient either to construct the receive system so that C is zero or to determine and subtract C from the Faraday angle measurements. Absolute phase angles, not just relative phase differences, are required to invert the bistatic radar data. Assuming that C has been accounted for through hardware construction or digital subtraction, the equation which remains then appears to be a backward difference approximation for the continuous quantity,

$$n(h) \propto \frac{d}{dh} \left\{ \frac{\cos[\phi(h)]}{\cos[\gamma(h)]} \theta(h) \right\}, \quad (4)$$

which gives the recipe for estimating electron density profiles from bistatic Faraday rotation. In practice, we associate altitudes and zenith angles with range gates using a formula which does not neglect the Earth's curvature, and then we evaluate (4) using a center difference method from the data with the help of the International Geomagnetic Reference Field (IGRF) 2000 magnetic field model [*Barton*, 1997].

The preceding discussion assumed that the signal was horizontally polarized immediately after scattering. In fact, the horizontally polarized transmitted signal will undergo Faraday rotation through an angle θ_j^i given by (3) prior to scattering, and immediately after scattering, the Faraday angle will therefore be $\theta_j' = 2\tan^{-1}[\tan(\theta_j^i/2)\cos(\xi_j)]$ (see discussion immediately following equation (1)). Consequently, the total Faraday angle measured by the receiver will be the sum of the parts incurred before, during, and after scattering:

$$\theta_j^{\text{tot}} = 2\tan^{-1}[\tan(\theta_j^i/2)\cos(\xi_j)] + \theta_j^r, \quad (5)$$

where the i and r superscripts refer to Faraday rotation accumulated strictly prior to and strictly after scattering. In a monostatic experiment, θ_j^i and θ_j^r will be equal and opposite in accordance with (2) but will add constructively and equally to the total observed Faraday angle θ_j^{tot}. In our bistatic experiments, θ_j^i and θ_j^r are equal and of the same sign but will contribute unequally to θ_j^{tot}, depending on the scattering angle. Whereas the θ_j^{tot} have been measured, the θ_j^r are required for the analysis outlined above. We therefore solve (5) iteratively in each range gate for θ_j^r and use the results to construct electron density profiles according to (4).

2.2. Azimuth Scatter

Figure 1 depicts scattering events occurring entirely in the plane containing the transmitter and the receiver and normal to the ground. In fact, the condition for coherent scatter is satisfied for ray paths with a large range of azimuth angles. Field-aligned backscatter arriving in a given range gate could originate from anywhere on a circular arc in the plane normal to the plane of Figure 1 and midway between the radars. The scattering altitude would be different at different points on the arc even though the range is the same. Only by severely limiting the range of possible azimuth angles involved in the experiment can we uniquely associate range with altitude and make the preceding analysis hold.

Azimuth scatter could be made negligibly small by using large antenna arrays with narrow beam widths. For the experiments in question we had available only small arrays comprised of four five-element Yagi antennas. However, the

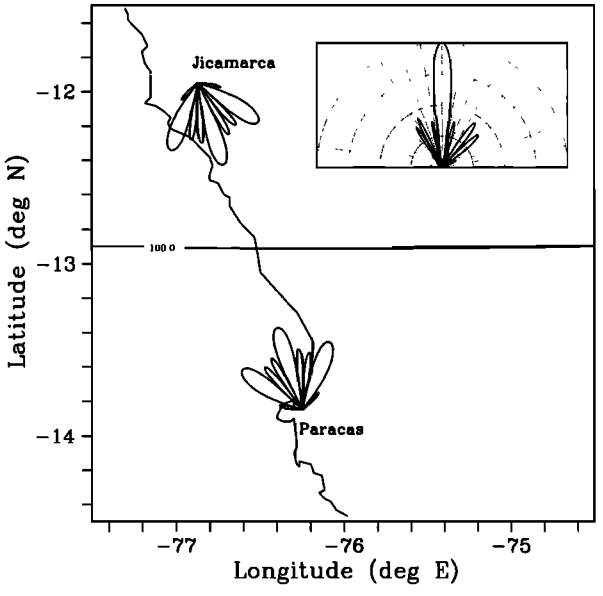

Figure 2. Geometry of the bistatic radar experiments. The irregular vertical curve is the Pacific coastline. The horizontal curve nearly bisecting the figure indicates the locus of perpendicularity at an altitude of 100 km. The inclination and declination of the magnetic field at the center of the scattering region are 0.65°and 0.68°, respectively. The radiation patterns for the Paracas and Jicamarca antennas are shown. (The origins of the patterns pinpoint the respective radar sites.) The inset shows the effective, two-way power pattern for the experiment as viewed from Jicamarca looking toward Paracas. Semicircles are drawn at 10-dB intervals.

unique geometry of the bistatic experiment makes it possible to achieve very narrow effective beam widths even with such modest antenna arrays.

Figure 2 shows the geometry of the Peruvian experiments. The horizontal lines represent the locus of perpendicularity for coherent scatter for different E and F region altitudes. Effectively, all scatter will arise from the nearly vertical plane containing these lines. Our strategy for achieving narrow main beam widths is to space the antennas in our arrays by distances much longer than one half-wavelength. Grating lobes result in the transmit and receive antenna patterns, but there need not be any grating lobes in the combined two-way power pattern.

Overlapping grating lobes can, in general, be avoided in bistatic radar experiments by using different, long antenna spacings at the transmit and receive sites. In the case of our experiments we used 3/2 wavelength spacing at both sites but still avoided grating lobes because of the particular magnetic field geometry. What makes this possible is the fact that points on the scattering plane defined by the locus of perpendicularity are not equidistant from the transmitter and the receiver except along the direct pointing azimuth. It is clear from Figure 2 that radiation emitted from the grating lobes of the Paracas array intercepts the scattering plane in such places that the scatter is strongly rejected by the Jicamarca array. The inset of Figure 2 shows the effective two-way power pattern of the combined arrays. The half-power full beam width of the main antenna beam is ~6°, and the sidelobes are down more than 20 dB.

In some circumstances, scatter from grating lobes might be tolerable so long as the range of the scatter is unambiguous. We maximize the sensitivity of our experiment by using a very high pulse repetition frequency. Consequently, suppressing grating lobe scatter is important here, since any sidelobe scatter would contribute to range-aliased clutter in the range gates of interest.

In practice, we correct for small amounts of residual azimuth scattering which otherwise affects the measurements above ~105-km altitude, where the signal-to-noise ratio starts to decrease rapidly with range and where the signal in a given range gate is apt to be contaminated by scatter from lower altitudes on the arc. The correction involves two steps. In the first step the appropriate shape function is deconvolved from the signal-to-noise ratio profile, the result being the profile that would be observed in the total absence of azimuth scattering. In the second step this profile is used to calculate the centroid scattering altitude $\langle h \rangle$ of the scatter falling into each range bin:

$$\langle h \rangle = \frac{\int h(s)P(s)ds}{\int P(s)ds},$$

where h is altitude, P is signal power, and the integration is over the arc equidistant from the transmitter and the receiver and associated with a given range gate. $P(s)$ is calculated theoretically on the basis of the signal-to-noise ratio profile and the antenna pattern. These centroid altitudes are then used when computing (4). The effects of azimuth scatter, which are mainly to yield anomalously small electron densities in the topside region, are thereby mitigated.

2.3. Practical Considerations

Although the antenna arrays give rise to a radiation pattern with a narrow main lobe and reduced sidelobes, they are inefficient in that much of the radiation is directed away from the ionospheric target. The sensitivity of the system is therefore somewhat compromised. Since the intent is to perform remote sensing of the ionosphere with small, low-cost radar systems, strategies for recovering sensitivity without turning to large antennas and transmitters are required. In part, the system sensitivity is improved by the fact that the scattering wavelength for bistatic scatter is somewhat longer than 3 m (~4.25 m in this case). The experiment therefore benefits, in comparison to a monostatic experiment, from the increased intensity of bottomside type II and topside pure two-stream irregularities at the longer wavelength. Likewise, since the antenna arrays are not directed upward, sky noise from the Milky Way is largely avoided.

Table 1 lists the parameters for the Faraday rotation experiment. We have used a short interpulse period to permit substantial incoherent integration and to fully utilize the duty cycle capabilities of the transmitter. At present, pulse coding is not possible with the Paracas transmitter system, although we hope to add coding capability. At Paracas, four five-element Yagi antennas are arranged in a broadside array and elevated at ~45°to the horizon. Two similar arrays, one for each linear polarization, have been installed at Jicamarca. In addition, the E planes of the Yagis at Jicamarca have been tilted ±45°so that approximately equal signal strengths are received by both linear polarizations. Tilting the antennas this way also symmeterizes ground effects and is important for achieving good impedance matches. Signals from the two polarized arrays are fed into a hybrid network made from coaxial cables to synthesize left and right circular polarizations. The circular polarizations are sampled by the Jicamarca data acquisition system. During data analysis the Faraday angle of the scatter is determined using correlation analysis.

Table 1. Bistatic Radar Operating Mode

Parameter	Value
Frequency, MHz	49.92
Scattering wavelength, m	4.25
Peak power, kW	20
Interpulse period, μs	250
Coherent integrations	8
Pulse width, μs	3
Range resolution, m	450
Range gates	40
Transmit coordinates	13.85°S, 76.25°W
Receive coordinates	11.95°S, 76.87°W
Antennas	four five-element Yagis 1.5 λ broadside spacing

2.4. Error Analysis

Volume scattering from ionospheric irregularities is a stochastic process, and the signals received by the radar possess the quality of Gaussian random variables even in the absence of background and instrument noise. Only the variances and covariances of these random variables have significance, and these must be estimated using various moment methods involving averages of a large number of observations. The stationarity of the random process is therefore always at issue. In contrast, the polarization angle of the scatter is deterministic and could, in principle, be determined from a single observation. In practice, the presence of background noise makes it necessary to perform averaging in Faraday rotation experiments as well. In the high-signal-to-noise level limit we nonetheless find that useful electron density profiles can be measured with only a few seconds of incoherent integration. The speed of this technique therefore exceeds, in some respects, that of incoherent scatter.

The data processing applied here is like that discussed in some detail by *Pingree* [1990]. Estimating the polarization angle from the power of signals received by two antenna arrays with crossed polarizations generally leads to poor results [*Farley*, 1969a; *Flood and Gamnitz*, 1965]. Instead, we use hybrid networks to synthesize signals corresponding to left and right circularly polarized waves, and we correlate them to determine the phase angle for each range gate. Methods of performing correlation analysis and estimating statistical variations are described by *Farley* [1969b] and others and will not be mentioned here. Having computed the complex cross-correlation function ρ for the two circular polarizations and determined from its real and imaginary parts the phase angle $\theta = \tan^{-1} \rho_i/\rho_r$, we can estimate its variance from *Bevington* [1969]:

$$\langle(\theta - \hat{\theta})^2\rangle = \langle(\rho_r - \hat{\rho}_r)^2\rangle \left(\frac{\partial\theta}{\partial\rho_r}\right)^2 + \langle(\rho_i - \hat{\rho}_i)^2\rangle \left(\frac{\partial\theta}{\partial\rho_i}\right)^2,$$

where the carets represent expected values and where errors in the real and imaginary parts of the correlation function are assumed to be uncorrelated. Further assuming that the variances of the real and imaginary parts of the correlation function contribute equally to its total variance, we find

$$\langle(\theta - \hat{\theta})^2\rangle \approx \frac{1}{2|\rho|^2}\langle|\rho - \hat{\rho}|^2\rangle.$$

Consequently, errors are minimized when the coherence of the left and right circularly polarized signals is high. Furthermore, the variance of the correlation function is itself a function of the coherence and, expressing $|\rho|^2 = 1 - \epsilon$, vanishes for large coherence as $\mathcal{O}(\epsilon)$ in the high-signal-to-noise limit [*Farley and Hysell*, 1996].

Two factors mainly limit coherence. The first is Faraday dispersion, a phenomenon associated with large variations in the absolute plasma density in the scattering volume defined by the pulse shape and the antenna pattern. Because of the low E region plasma densities involved, the narrow beam width of the bistatic radar, and the short pulse lengths involved, Faraday dispersion is not expected to be problematic in these experiments. The other factors limiting coherence are noise and interference. (Note that the coherence quantity described here is not one that is normalized for noise.) To the extent that noise alone is responsible for decorrelation of the circularly polarized signals, $|\rho| = S/(S + N)$ and the variance of the correlation function becomes

$$\langle|\rho - \hat{\rho}|^2\rangle \approx \frac{1}{K}\left(\frac{N}{S} + \frac{3}{2}\frac{N^2}{S^2}\right),$$

where K is the number of statistically independent samples used to estimate the correlation function. Since the correlation time of the echoes is on the order of 5 ms, K will typically be on the order of 10^4 to 10^5 for these experiments. Given incoherent integration times on the order of minutes, we find that Faraday angles of sufficient accuracy for estimating electron density profiles can be measured in range bins where the signal-to-noise ratio is of order unity or greater.

Note that additional, systemic errors are introduced into the experiment by cross talk, the lack of independence of the two received signals. Cross talk is caused by slightly improper alignment of the receiving antennas, by imperfections in the cabling, and by communication between the receiver channels in the receiver and data acquisition electronics. Cross talk leads to biases in the Faraday angle measurement and, in the long run, to distorted density profile estimates. The effects of cross talk were analyzed in detail by *Farley* [1969a] and *Pingree* [1990]. Methods for suppressing first- and second-order cross talk have been devised for use with incoherent scatter experiments performed at Jicamarca. These depend on phase-flipping schemes requiring the ability to control the transmitted right and left circularly polarized waves independently. Our system does not possess that capability at present but should in the future. For now we recognize that the Faraday angle measurements to be presented may possess subtle but spurious features.

3. Data Presentation

Experiments were performed on September 12–13 and November 10–12, 2000. For all the experiments the transmit and receive stations at Paracas and Jicamarca, respectively, were synchronized using GPS receivers. The observations were qualitatively similar, and we concentrate here on data from September 12, when the midday echoes were strongest. Those echoes have been plotted in range-time-intensity (RTI) format in Figure 3a. Only signal levels above 5 dB are shown in order to emphasize the contrast, but signals well below -10 dB were registered accurately. The altitude extent of this scattering layer is typical for the daytime electrojet under strong driving conditions, and indication that azimuth scatter has, indeed, been mainly suppressed. Vertical streaks throughout the RTI plot indicate the presence of sporadic but strong radio interference.

The echoes depicted in Figure 3a and others detected with the bistatic radar are qualitatively similar to those observed in conventional monostatic coherent scatter experiments performed at Jicamarca and elsewhere [*Kudeki et al.*, 1987;

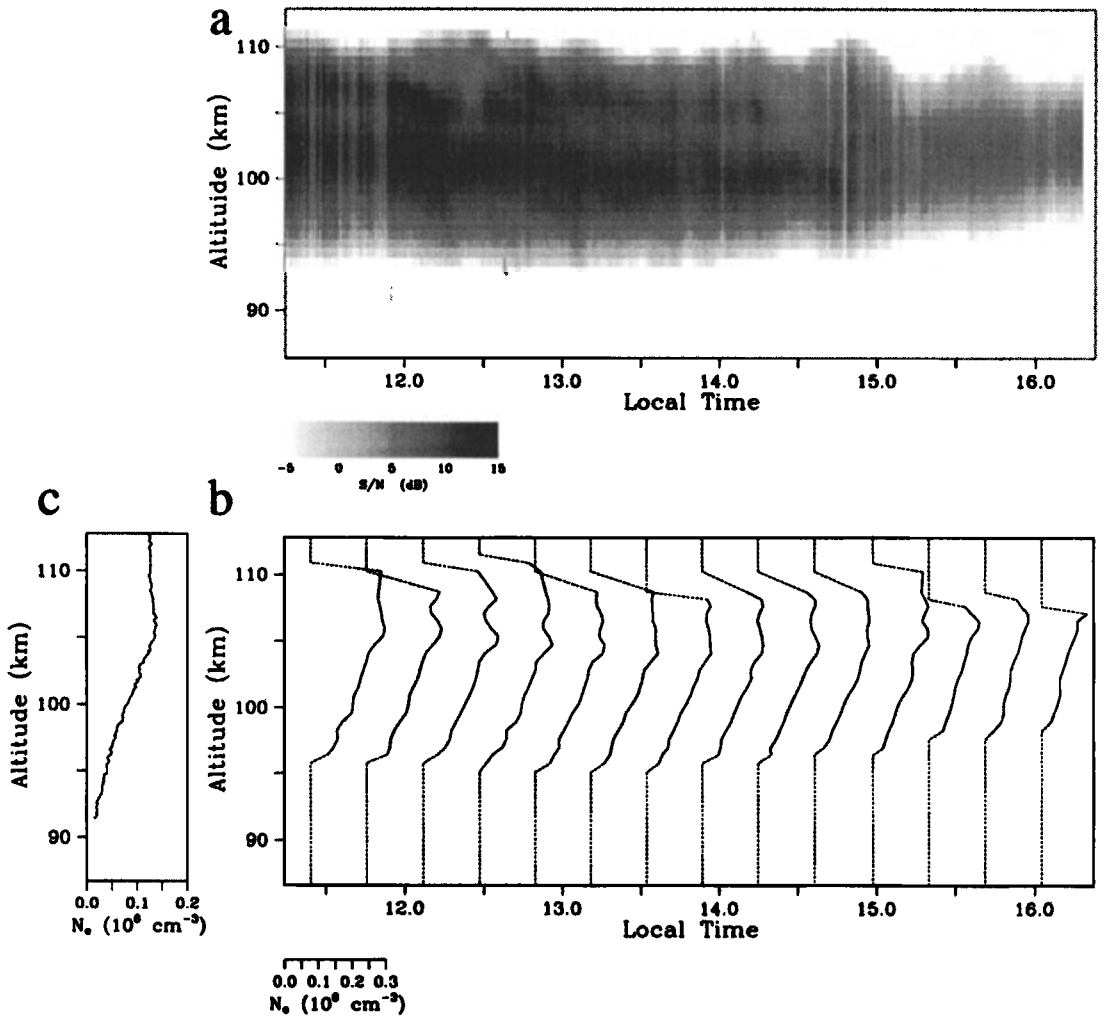

Figure 3. (a) Range time intensity plot for September 12, 2000. (b) Corresponding electron density profiles computed at ~20-min. intervals using Faraday rotation analysis. Only measurements with sufficiently small error bars are shown. Dashed lines help to identify the midpoint time of the data integration. (c) Electron density profile measured with a sounding rocket during the Condor campaign in Peru on March 12, 1983, at 1034 LT [after *Pfaff et al.*, 1985].

Pfaff et al., 1987b; *Kudeki and Farley*, 1989]. Strong echoes are evident below ~105 km, the nominal altitude of the daytime *E* region density peak, where gradient drift turbulence is expected to form. Moreover, topside echoes sometimes appear in mid afternoon as well. The RTI plot in Figure 3 shows a strong, secondary scattering layer between ~107-110 km altitude, precisely the range of altitudes where the electrojet current is generally strongest, which persists until ~1500 LT. Such scattering layers are often but not always evident in our bistatic data around midday and were strongest and most persistent on September 12.

Kudeki et al. [1987] explained the existence of such scattering layers, which form in the topside *E* region where the gradient drift mechanism is stable during the daytime, in terms of a pure two-stream process. Nonlinear three-wave interactions involving the beating of two horizontally propagating, linearly unstable two-stream waves producing a third, vertically propagating, linearly stable wave were proposed to account for the topside echoes, which have small Doppler shifts in accordance with the three-wave resonance conditions. Additional evidence for this mechanism includes the fact that secondary two-stream waves, indicators of kilometer-scale gradient drift waves in the electrojet, disappear in the topside region as well as the fact that the topside echoes are less aspect sensitive than bottomside echoes, in accordance with expectations for an inverse cascade [*Kudeki and Farley*, 1989]. Furthermore, *Pfaff et al.* [1987b] observed a laminar layer of horizontally propagating two-stream waves centered at 108-km altitude in rocket data from the Condor equatorial electrojet campaign. Embedded in this topside layer were vertically propagating waves with characteristics consistent with the inverse cascade hypothesis. The existence of pure two-stream waves in the daytime electrojet is important for the present study since they offer a means of measuring the electron density profile in the topside, which would otherwise be invisible to coher-

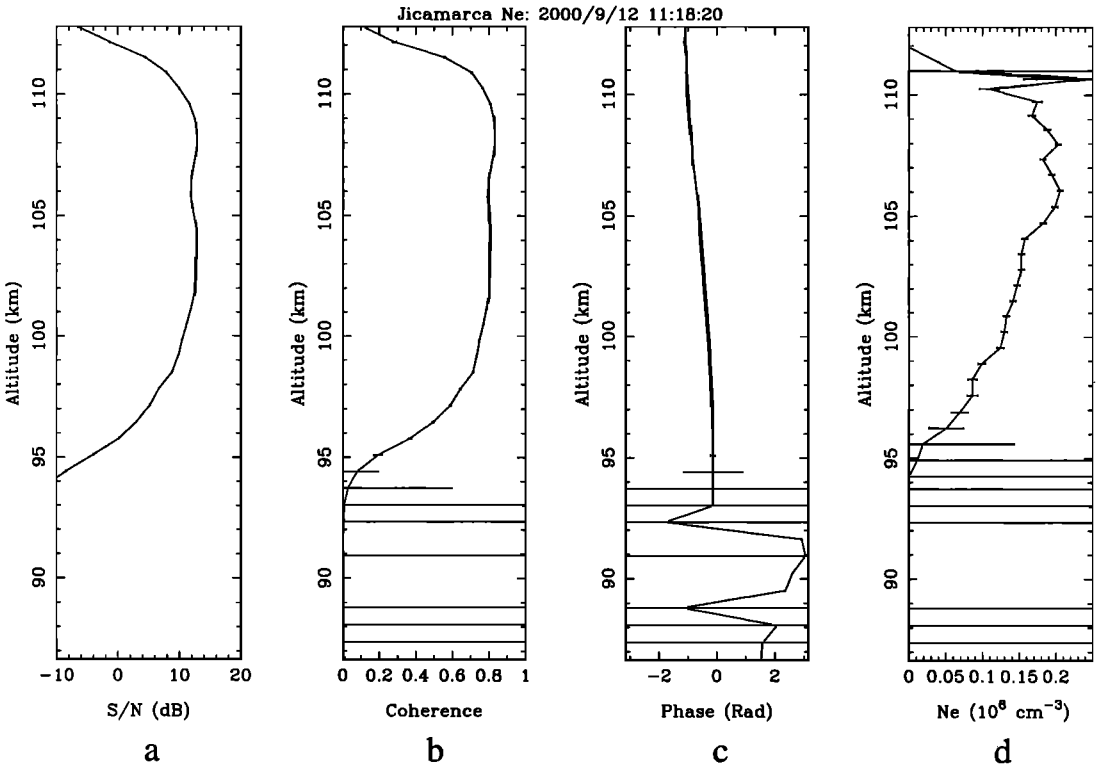

Figure 4. Bistatic electrojet scatter analysis: (a) signal-to-noise ratio, (b) signal coherence, (c) Faraday angle, and (d) plasma density, as functions of altitude. The incoherent integration time for this plot was 5 min. Error bars reflect the theoretical expected variances.

ent scatter radars. Reversing the argument, our experiments are useful here since they demonstrate unambiguously that small-scale plasma irregularities can be produced in the daytime on the topside. Furthermore, since the topside waves are produced by an inverse cascade, they are ideal for detection by the bistatic technique which probes wavelengths at the outer scale of two-stream turbulence.

Figure 4 presents results from the Faraday rotation analysis. Figures 4a - 4d show the signal-to-noise ratio, the coherence (magnitude of correlation) of the left and right circular polarizations, the phase angle, and the electron density inferred according to (4), respectively. The vertical axes represent altitude. Note that the phase angles in Figure 4c are the inferred angles θ_j^r described in section 2.1, which represent phase rotations taking place strictly on the return path and which are derived from the measured phase angles θ_j^{tot}. The altitudes of the electron density estimates in Figure 4d, meanwhile, correspond to the centroid scattering altitudes described at the end of section 2.2. The incoherent integration time for Figure 4 was 5 min. Additional incoherent integration could be used to recover more useful data points at lower altitudes at the expense of coarser time resolution. The density profile in Figure 4 has a peak density of $\sim 2 \times 10^5$ cm^{-3}. The peak occurs at an altitude of $\sim$105 km and corresponds to the depression in the signal-to-noise ratio between the bottomside scattering layer and the pure two-stream topside layer.

Figure 3b shows a succession of inferred electron density profiles (solid lines) like the one from Figure 4d except computed using 20-min. incoherent integrations. (Much finer time resolution is possible at the expense of the accuracy of the measurements at the extremes of the profiles.) Data points with error bars of less than 4×10^4 cm^{-3} are plotted with solid lines connecting them. Dashed lines are used to help associate the curves with the midpoint times of the data integrations. The profiles illustrate the behavior of the E region from before noon into late afternoon. They have been plotted beneath the RTI map in order to aid comparisons between structure in the backscatter intensity and layer density.

Here and in observations made on other days, regions in the bottomside where the vertical density gradient is steepest generally coincide with regions of strongest backscatter intensity. In the topside where the density profiles sometimes exhibit subtle structuring, enhancements in the scattering are also evident where the density profile has a positive gradient. The structuring in question has the form of a noticeable bump at the peak along with additional layering that can persist for intervals of an hour or more. This layering becomes more obvious when shorter incoherent integration times are used and is coincident with sporadic structure in the topside in the RTI plot. At times, gradient drift turbulence may have been excited above 105 km and contributed to the backscatter. The peak in the profiles evident here descends until $\sim$1330 LT, when it begins to rise. More diffuse echoes from the topside are detected until $\sim$1500 LT. Afterward, scattering appears to cut off for altitudes above the electron density peak, signifying that the conditions for primary two-stream wave instability have ceased. Similar

remarks hold for the other bistatic radar datasets. Electrojet observations were made on September 13 until ~1700 LT when poor signal strength prevented the accurate determination of Faraday angles and electron densities. Strong echoes starting at sunrise and persisting until sunset were observed in the November experiments, but no useful nighttime data have been acquired thusfar.

For comparison we plot in Figure 3c an electron density profile measured by *Pfaff et al.* [1985] with an instrumented sounding rocket flown from Peru on March 12, 1983, during the Condor campaign. These are the most recent observations of their kind from the Peruvian sector. They were taken at 1034 LT, ~1 hour earlier in LT than the earliest radar-derived profile we show. If one were to superimpose this profile on the earliest few radar-derived profiles, one would find that the profile shapes match quite closely. A density peak at ~105 km, a plateau above that, and a steep decrease in density below the peak are common to the radar and rocket measurements. However, the peak density observed by the rocket was only $\sim 1.4 \times 10^5$ cm^{-3} versus $\sim 2.0 \times 10^5$ cm^{-3} for the radar. The difference is attributable, in part, to the difference in local time and, more importantly, to the difference in the phase of the solar cycle. It is noteworthy that the four electron density profiles measured off the coast of Peru on different days near local noon in March of 1965 by *Aikin and Blumle* [1968] have characteristics similar to the rocket data shown here. The profiles varied from day to day only in their small details. The local time coverage of the entire sounding rocket database is too poor for meaningful comparison with the radar data.

The IRI model [*Bilitza et al.*, 1993] was used to generate model E region density profiles for the location, year, season, and local times of our measurements. The model predicts peak noontime densities of $\sim 1.9 \times 10^5$ cm^{-3} at altitudes between 105 and 110 km, decreasing to $\sim 1.0 \times 10^5$ cm^{-3} by 1600 LT. These peak density predictions are closely matched by the Faraday rotation data throughout the whole afternoon of September 12, 2000. However, the IRI model does not predict very accurately the shape of the radar-derived profiles. Fine structure is obviously absent from the model profiles. Moreover, model densities do not exhibit a clear peak near 105-km altitude and tend to decline much more slowly with decreasing altitude below 105 km than do the radar-derived profiles. Similar remarks hold for comparisons between much of the rocket data from Peru and IRI model runs for appropriate solar cycle conditions. On the basis of the limited data discussed here, it appears that the IRI model cannot reproduce very accurate daytime equatorial E region density profile shapes but does provide relatively accurate peak density estimates. Additional Faraday rotation observations will reveal the extent to which empirical models of the equatorial E region require updating.

4. Summary and Conclusions

Information about the equatorial E region plasma density profile has come mainly from campaigns involving instrumented sounding rockets. Rocket experiments provide a detailed but brief and only occasional glimpse of this region of the ionosphere. The unavailability of remote sensing data from this region hinders several lines of research in equatorial aeronomy and plasma physics. These include studies of the equatorial electrojet current system, of the plasma irregularities and instabilities that form in the electrojet, and of low-latitude ionospheric electrodynamics. Along with existing and emerging methods for measuring the polarization electric field and the neutral wind profile in the electrojet, the technique described here offers a means of collecting some of the same information gathered by sounding rockets on a regular basis by exploiting coherent scatter [*Chau et al.*, 2000; *Hysell and Burcham*, 2000; *Tsunoda et al.*, 2000].

The shapes of the daytime density profiles presented here are similar to those of profiles measured in situ near local noon, and the peak densities observed agree with IRI model predictions throughout the day. Subtle, periodic layering in the daytime profiles not generally seen by sounding rockets is sometimes observed in the Faraday rotation data. More experimentation, analysis, and validation is required to determine if this feature is genuine or an artifact of residual azimuth scattering or cross talk. The IRI model does not appear to reproduce the shapes of either the radar or the rocket measurements closely, but the technique described here provides a means of updating the model. New observations spanning a variety of local times, seasons, and points in the solar cycle are clearly needed to expand the empirical database. We plan to make more observations and also to increase the sensitivity of the experiment to facilitate the measurement of nighttime density profiles. The nighttime equatorial E region is one of the most poorly characterized, least probed regions of the ionosphere, but the in situ data available show that it is highly structured and dynamic [*Prakash et al.*, 1972; *Larsen and Odom*, 1997]. The technique introduced here could provide useful estimates of E region plasma densities below 1×10^4 cm^{-3} given integration times of tens of minutes wherever signal-to-noise ratios in excess of unity are detected.

Finally, applicability of this technique is not limited to the equatorial zone. So long as the conditions for Bragg scatter are satisfied, the experiment described here could be applied at midlatitudes toward investigations of sporadic E layers and quasiperiodic echoes. Likewise, at high latitudes, where range is related more to the horizontal distance to the target than to altitude, the bistatic Faraday rotation experiment could utilize auroral electrojet echoes to probe the structure of the auroral oval, blobs, and patches. While this paper has concentrated in E region coherent echoes, F region coherent echoes could also be exploited. The technique may provide a means of obtaining F region density profiles when spread F prevents ionogram inversion.

Acknowledgments. The experiments reported here were made possible by the staff of the Jicamarca Radio Observatory and especially by R. F. Woodman, who allowed us to use his home in Paracas and who also made several important suggestions. This work was supported by the National Science Foundation through cooperative agreements ATM-9022717 and ATM-9408441 to Cornell University and by NSF grant ATM-9978792 to Clemson University. The Jicamarca Radio Observatory is operated by the Geophysical Institute of Peru, Ministry of Education, with support from the NSF cooperative agreements just mentioned.

Janet G. Luhmann thanks C. A. Reddy and Wesley E. Swartz for their assistance in evaluating this paper.

References

Aikin, A. C., and L. J. Blumle, Rocket measurements of the *E* region electron concentration distribution in the vicinity of the geomagnetic equator, *J. Geophys. Res.*, *73*, 1617, 1968.

Aponte, N., R. F. Woodman, W. E. Swartz, and D. T. Farley Measuring ionospheric densities, temperatures, and drift velocities simultaneously at Jicamarca, *Geophys. Res. Lett.*, *24*, 2941, 1997.

Barton, C. E., International Geomagnetic Reference Field: The seventh generation, *J. Geomagn. Geoelectr.*, *49*, 123, 1997.

Bevington, P. R., *Data Reduction and Error Analysis for the Physical Sciences*, McGraw-Hill, New York, 1969.

Bilitza, D., K. Rawer, L. Bossy, and T. Gulyaeva, International Reference Ionosphere: - Past, present, future, *Adv. Space Res.*, *13*, 3, 1993.

Booker, H. G., *Cold Plasma Waves*, Martinus Nijhoff, Zoetermeer, Netherlands, 1984.

Budden, K. G., *The Propagation of Radio Waves*, Cambridge Univ. Press, New York, 1988.

Chau, J. L., D. T. Farley, and B. B. Balsley, East-west asymmetry in type 1 electrojet echoes at Jicamarca, paper presented at X International Symposium on Equatorial Aeronomy, Antalya, Turkey, May 17–23, 2000.

Farley, D. T., Faraday rotation measurements using incoherent scatter, *Radio Sci.*, *4*, 935, 1969a.

Farley, D. T., Incoherent scatter correlation function measurements, *Radio Sci.*, *4*, 935, 1969b.

Farley, D. T., and D. L. Hysell, Radar measurements of very small aspect angles in the equatorial ionosphere, *J. Geophys. Res.*, *101*, 5177, 1996.

Fesen, C. G., R. G. Roble, A. D. Richmond, G. Crowley, and B. G. Fejer, Simulation of the pre-reversal enhancement in the low latitude vertical ion drifts, *Geophys. Res. Lett.*, *27*, 1851, 2000.

Flood, W. A., and H. G. Gamnitz, Faraday rotation and volume scatter, *J. Geophys. Res.*, *70*, 4391, 1965.

Forbes, J. M., The equatorial electrojet, *Rev. Geophys.*, *19*, 469, 1981.

Hysell, D. L., and J. Burcham, Ionospheric electric field estimates from radar observations of the equatorial electrojet, *J. Geophys. Res.*, *105*, 2443, 2000.

Jackson, J. D., *Classical Electrodynamics* (2nd ed.), John Wiley, New York, 1975.

Kudeki, E., and D. T. Farley, Aspect sensitivity of equatorial electrojet irregularities and theoretical implications, *J. Geophys. Res.*, *94*, 426, 1989.

Kudeki, E., B. G. Fejer, D. T. Farley, and C. Hanuise, The Condor equatorial electrojet campaign: Radar results, *J. Geophys. Res.*, *92*, 13,561, 1987.

Larsen, M. F., and C. D. Odom, Observations of altitudinal and latitudinal *E*-region neutral wind gradients near sunset at the magnetic equator, *Geophys. Res. Lett.*, *24*, 1711, 1997.

Pfaff, R. F., Rocket observations of the equatorial electrojet: Current status and critical problems, *J. Atmos. Terr. Phys.*, *53*, 709, 1991.

Pfaff, R. F., M. C. Kelley, B. G. Fejer, N. C. Maynard, L. G. Brace, B. G. Ledley, L. G. Smith, and R. F. Woodman, Comparitive in situ studies of the unstable daytime equatorial *E* region, *J. Atmos. Terr. Phys.*, *47*, 791, 1985.

'faff, R. F., M. C. Kelley, E. Kudeki, B. G. Fejer, and K. D. Baker, Electric field and plasma density measurements in the strongly driven daytime equatorial electrojet, 1, The unstable layer and gradient drift waves, *J. Geophys. Res.*, *92*, 13,578, 1987a.

Pfaff, R. F., M. C. Kelley, E. Kudeki, B. G. Fejer, and K. D. Baker, Electric field and plasma density measurements in the strongly driven daytime equatorial electrojet, 2, Two-stream waves, *J. Geophys. Res.*, *92*, 13,597, 1987b.

Pfaff, R. F., J. H. A. Sobral, M. A. Abdu, W. E. Swartz, J. W. LaBelle, M. F. Larsen, R. A. Goldberg, and F. J. Schmidlin, The Guará campaign: A series of rocket-radar investigations of the Earth's upper atmosphere at the magnetic equator, *Geophys. Res. Lett.*, *24*, 1663, 1997.

Pingree, J. E., Incoherent scatter measurements and inferred energy fluxes in the equarotial *F*-region ionosphere, Ph.D. thesis, Cornell Univ., Ithaca, N. Y., 1990.

Prakash, S., B. H. Subbaraya, and S. P. Gupta, Rocket measurements of ionization irregularities in the equatorial ionosphere at Thumba and identification of plasma irregularities, *Indian J. Radio Space Phys.*, *72*, 1, 1972.

Ratcliffe, J. A., *The Magneto-Ionic Theory and its Applications to the Ionosphere*, Cambridge Univ. Press, New York, 1959.

Ratcliffe, J. A., *An Introduction to the Ionosphere and Magnetosphere*, Cambridge Univ. Press, New York, 1972.

Ronchi, C., Large scale turbulence in the equatorial electrojet, Ph.D. thesis, Cornell Univ., Ithaca, N. Y., 1990.

Tsunoda, R. T., W. L. Ecklund, and P. E. Johnston, Radar measurements of electric fields in the topside of the equatorial electrojet: First results, *Geophys. Res. Lett.*, *27*, 2861, 2000.

Woodman, R. F., Equatorial ionospheric irregularities as observed by the Jicamarca radar, paper presented at Colloquium on Low-Latitude Ionospheric Physics, Comm. on Space Programs and Res., Taipei, Taiwan, 1994.

J. L. Chau, Radio Observatorio de Jicamarca, Instituto Geofísico del Perú, Lima 13, Perú.

D. L. Hysell, Department of Physics and Astronomy, Clemson University, Clemson, SC 29634-1911. (dhysell@clemson.edu)

(Received December 15, 2000; revised April 2, 2001; accepted April 2, 2001.)